magnetochemistry

MDPI

Article

Giant Angular Nernst Effect in the Organic Metal α-(BEDT-TTF)$_2$KHg(SCN)$_4$

Danica Krstovska [1,*], Eun Sang Choi [2] and Eden Steven [2,3]

[1] Faculty of Natural Sciences and Mathematics, Ss. Cyril and Methodius University, Arhimedova 3, 1000 Skopje, North Macedonia
[2] National High Magnetic Field Laboratory, Florida State University, 1800 E. Paul Dirac Drive, Tallahassee, FL 32310, USA
[3] Emmerich Research Center, Jakarta Utara DKI, Jakarta 14450, Indonesia
* Correspondence: danica@pmf.ukim.mk

Abstract: We have detected a large Nernst effect in the charge density wave state of the multiband organic metal α-(BEDT-TTF)$_2$KHg(SCN)$_4$. We find that apart from the phonon drag effect, the energy relaxation processes that govern the electron–phonon interactions and the momentum relaxation processes that determine the mobility of the q1D charge carriers have a significant role in observing the large Nernst signal in the CDW state in this organic metal. The emphasised momentum relaxation dynamics in the low field CDW state (CDW$_0$) is a clear indicator of the presence of a significant carrier mobility that might be the main source for observation of the largest Nernst signal. The momentum relaxation is absent with increasing angle and magnetic field, i.e., in the high-field CDW state (CDW$_x$) as evident from the much smaller Nernst effect amplitude in this state. In this case, only the phonon drag effect and electron–phonon interactions are contributing to the transverse thermoelectric signal. Our findings advance and change previous observations on the complex properties of this organic metal.

Keywords: Nernst effect; organic metal; charge density wave; quantum oscillations; relaxation processes

Citation: Krstovska, D.; Choi, E.S.; Steven, E. Giant Angular Nernst Effect in the Organic Metal α-(BEDT-TTF)$_2$KHg(SCN)$_4$. *Magnetochemistry* **2023**, *9*, 27. https://doi.org/10.3390/magnetochemistry9010027

Academic Editors: Laura C. J. Pereira and Dulce Belo

Received: 8 December 2022
Revised: 3 January 2023
Accepted: 7 January 2023
Published: 10 January 2023

1. Introduction

Thermoelectric effects provide an important information concerning the sign of the transport carriers and may be useful for the study of the relation between the anisotropy of the electronic bands and superconducting state, especially in multiband superconductors. It is well known that measurements of the Seebeck effect (which is a longitudinal voltage induced by a temperature gradient in a magnetic field) as a function of temperature yield important information concerning not only parameters of charge carriers but also the nature of the electron–phonon scattering in the system, which is especially important for a class of materials such as are organic layered conductors, where strong Fermi liquid effects have been anticipated. The Nernst effect, which is an analogue of the Hall effect, is the transverse voltage induced by a temperature gradient in a magnetic field. It is considered as an important probe of strongly correlated electron systems. The Nernst effect was discovered in bismuth, and experimental studies have shown that it is the dominant thermoelectric response in this material [1]. The Nernst effect is usually small in normal metals, but it is large in semimetals. In high-T_c cuprates, a large Nernst effect was observed in the vicinity of the resistive transition temperature T_c [2] and also near the mobility edge [3]. A giant resonant Nernst signal was also discovered in some layered organic conductors such are the quasi one-dimensional (q1D) organic conductors (TMTSF)$_2$PF$_6$ [4,5] and (TMTSF)$_2$ClO$_4$ [6]. In the former, a giant Nernst effect was detected in tilted magnetic fields near the Lebed magic angles parallel to crystallographic planes. In the latter, a Nernst effect with a greatly enhanced amplitude was found not only in the metallic state but also at high fields in the field-induced spin density wave state. For what concerns the

quasi-two dimensional (q2D) organic conductors, the magnetoresistance, Hall resistance and magnetisation have been studied in detail in many compounds [7]. However, the thermoelectric response which yields information about both the thermodynamic and transport properties of charge carriers has been less investigated. The q2D character of the electron energy spectrum of layered organic conductors distinguishes them from both the two-dimensional materials and normal metals. While the magnetoresistance and Hall effect studies were successfully utilized for the Fermi surface (FS) reconstruction of organic conductors and enabled obtaining important information about the charge carriers, the investigation of the thermoelectric effects (especially in strong magnetic fields) allows us to obtain additional insights about the structure of the electron energy spectrum, as these effects are much more sensitive to the changes in the energy spectrum. The thermoelectric effects are also important for revealing the presence of the q1D FS open sheets in multiband organic conductors.

In this work, we investigate the Nernst effect behaviour in a quasi-two dimensional, two-band organic metal α-(BEDT-TTF)$_2$KHg(SCN)$_4$. This organic conductor has been an object of intense experimental studies for many years due to its unusual electronic properties (see Ref. [8] and references therein). The FS consists of both a q2D cylinder and a pair of weakly warped open q1D sheets. The q1D and q2D bands are separated by a substantial gap near the Fermi level. At T_p = 8 K, the system undergoes a phase transition from metallic to a charge density wave (CDW) state due to the nesting of the q1D open sheets. At the kink field B_K, the low-field CDW$_0$ state is transformed into the high-field CDW$_x$ state with a field-dependent wavevector. Throughout the years, there have been many reports on the magnetotransport studies at low temperatures in this organic metal aiming to obtain information on the Fermi surface topology as well as to explain the origin of the charge density wave state at temperatures below $T_p = 8$ K [9–13]. On the contrary, the thermoelectric transport has not been studied in much detail. In that regard, our goal is to make a contribution to the investigation of the thermoelectric response in the given compound, especially at low temperatures. Our studies show that at low temperatures, in α-(BEDT-TTF)$_2$KHg(SCN)$_4$, the thermoelectric response is mainly off-diagonal, although both Seebeck and Nernst effect are detected. We have detected a giant angular resonant Nernst effect in the CDW state of α-(BEDT-TTF)$_2$KHg(SCN)$_4$ similar to that reported in some q1D organic compounds. Furthermore, the magnetic field dependence of the Nernst effect reveals a resonant-like behaviour with sign change at certain magnetic fields when the magnetic field is tilted at the magic angles. The temperature dependence reveals that the relaxation processes have a significant role in the observed large Nernst effect in this compound. It also shows and confirms previous observations that in α-(BEDT-TTF)$_2$KHg(SCN)$_4$, there are different phases existing within a given temperature interval.

2. Materials and Methods

The single-crystal sample in this study was grown using conventional electrochemical crystallization techniques and was mounted on a rotating platform. Au wires were attached to the sample along the *b*-axis and on the edges of the *ac*-plane of the sample by carbon paste for both the resistance and Nernst effect measurements, respectively (Figure 1). The resistance was measured by a conventional 4-probe technique. The sample was positioned between two quartz blocks, which were heated by sinusoidal heating currents with an oscillation frequency f_0 and phase difference of $\pi/2$ to establish a small temperature gradient along the *b*-axis. The details about the method used for the thermoelectric measurements are given in Ref. [14]. The direction of the magnetic field is arbitrary, $\mathbf{B} = (B\sin\theta\cos\phi, B\sin\theta\sin\phi, B\cos\theta)$, where θ is the polar angle (measured from the *b*-axis to *ac*-plane) and $\phi = 37^\circ$ is the azimuthal angle (measured from the *c*-axis in the *ac*-plane).

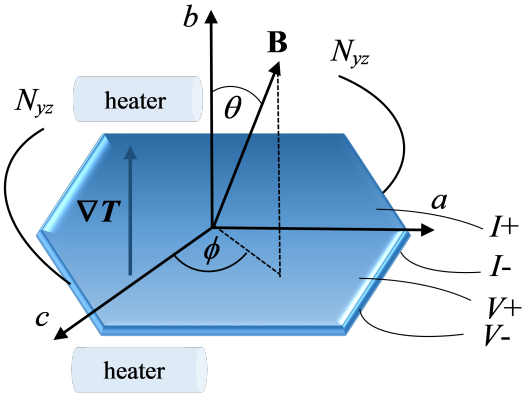

Figure 1. The experimental setup for the Nernst effect measurements as a function of the magnetic field strength and orientation. The temperature gradient ∇T is along the less conducting axis, *b*-axis of the conductor, perpendicular to the Q2D conducting *ac* plane. The magnetic field **B** is rotated for angle θ from the *b*-axis to the *ac*-plane at a fixed azimuthal angle of $\phi = 37^\circ$ from the *c*-axis.

3. Results and Discussion

In the following, we present a detailed study of the Nernst effect in the multiband organic conductor α-(BEDT-TTF)$_2$KHg(SCN)$_4$ with the magnetic field magnitude, orientation and temperature. The magnetic field and angular dependencies are obtained in the low-temperature regime in the CDW state of the conductor. The Nernst effect investigation allows us to obtain more insights about the behaviour of different CDW states that develop in this conductor as well as information on the driving mechanism for the CDW instabilities in α-(BEDT-TTF)$_2$KHg(SCN)$_4$. Additionally, it may give information about the role of quasiparticles in the transport processes in multiband systems.

3.1. Angular Hall and Nernst Effect Oscillations

The angular Hall resistance oscillations (AHROs) in the CDW$_0$ state of α-(BEDT-TTF)$_2$ KHg(SCN)$_4$ are shown in Figure 2 for several fields: 10 T, 15 T, and 21 T at $T = 0.6$ K. The Hall resistance quantum oscillations, associated with the Landau quantization of the closed FS orbit, are observed superimposed on the angular oscillations for each magnetic field strength. Although in the CDW phase, no q1D FS open sheets should survive, there appear clear angle-dependent Hall resistance oscillations similar to the Lebed resonances, which are characteristic for q1D organic conductors [15]. The AHRO maxima and minima appear at angles $\theta_{\mathrm{max}i}$ and $\theta_{\mathrm{min}i}$ where $i = 1, 2, 3, \ldots$. Interestingly, the dips in the Hall resistance become sharp at angles above $\theta = 60^\circ$, whereas the first minimum occurring at $\theta_{\mathrm{min1}} \sim 45^\circ$ is rather broad especially with increasing magnetic field magnitude. This is in contrast to the angular magnetoresistance oscillations (AMROs) behaviour in α-(BEDT-TTF)$_2$KHg(SCN)$_4$ (see Figure 2) where the maxima in the angular dependence are not as sharply pronounced as those in the AHROs. The Hall resistance is negative, indicating that in α-(BEDT-TTF)$_2$KHg(SCN)$_4$, the in-plane transport is mainly electron-like independently on the field direction with respect to the layers. An important observation is that the AHRO maxima occur at angles at which AMRO minima appear known as Lebed magic angles. Consequently, AHRO minima are observed at angles at which AMRO maxima are detected. However, there is a slight shift between the AMRO (AHRO) maxima (minima) seen only at angles below $\theta = 60^\circ$. This can be more clearly identified from the corresponding curves presented in Figure 3 below. With rotation of the magnetic field toward the plane of the layers, more charge carriers have been involved in the transport processes, which can account for the absence of a shift between the AMRO (AHRO) maxima (minima) at angles above $\theta = 60^\circ$. Interestingly, changes in the angle-dependent Nernst effect also occur around this angle at each magnetic field magnitude. Our results show that in the compound under consideration, the thermoelectric transport is more complex than previously anticipated, as the large Nernst signal arises in total absence of superconducting

fluctuations. This opens a new window for investigation of the driving mechanism for the CDW instabilities in α-(BEDT-TTF)$_2$KHg(SCN)$_4$.

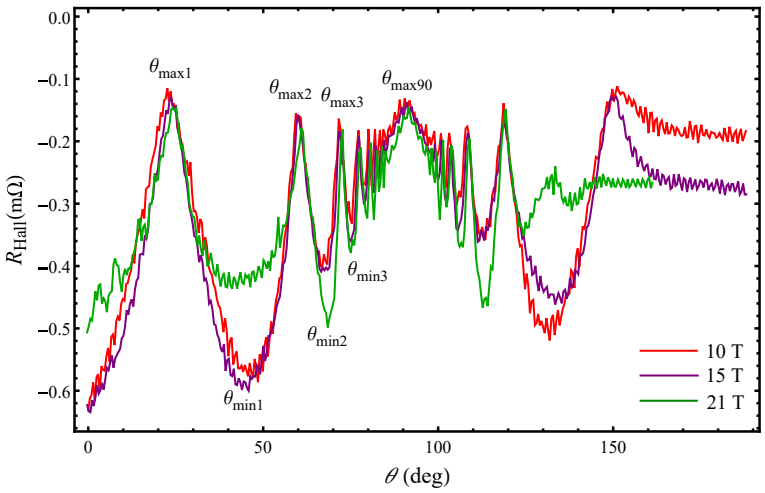

Figure 2. Angular oscillations of the Hall resistance in α-(BEDT-TTF)$_2$KHg(SCN)$_4$ for several fields: $B = 10$ T, 15 T, 21 T at $T = 0.6$ K. The quantum oscillations are visible at each field magnitude in the whole range of angles. The positions of some of the AHROs maxima and minima are indicated.

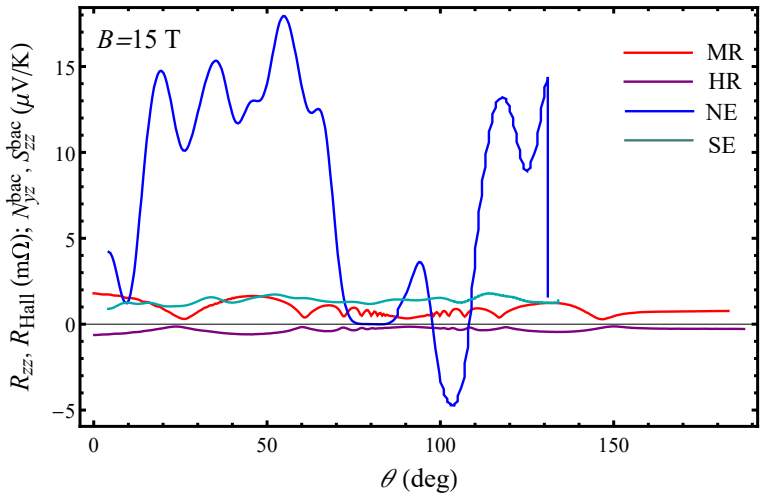

Figure 3. Comparison of the angular dependence of magnetoresistance, Hall resistance, Seebeck and Nernst effect in α-(BEDT-TTF)$_2$KHg(SCN)$_4$ for $B = 15$ T and $T = 0.6$ K. The Nernst effect amplitude is extremely large compared to the amplitude of magnetoresistance, Hall resistance and thermopower in a wide range of angles with exception of the angles near the plane of the layers.

We present in Figure 4 the angular dependence of the total Nernst effect in α-(BEDT-TTF)$_2$KHg(SCN)$_4$ for several fields: $B = 10$ T, 23 T, 26 T and 30 T at $T = 0.6$ K. We have detected an angular Nernst signal with a large amplitude for each magnetic field magnitude. Exceptions from this are certain angles as discussed below. We find that in α-(BEDT-TTF)$_2$KHg(SCN)$_4$, the angular Seebeck effect (thermopower) [16] is much smaller than the Nernst effect, although the thermoelectric measurements are performed for a longitudinal temperature gradient. Both effects show oscillations, but the transverse component is clearly dominant, as it is about 10 times larger than the longitudinal one. This is also a case even for magnetic field orientations close to the less conducting axis (b-axis) where the thermopower is expected to be the dominant thermoelectric response. The rather complex nature of the observed angular Nernst signal in α-(BEDT-TTF)$_2$KHg(SCN)$_4$ is correlated with its multiband character as two kinds of carriers are involved in the thermoelectric transport. The giant Nernst effect previously observed in some of the

q1D organic compounds with an undetectable Seebeck effect has been ascribed to the vortex flow [4,5]. On contrary, the superconducting state in α-(BEDT-TTF)$_2$KHg(SCN)$_4$ develops below $T_c = 0.1$ K and for a quasi-hydrostatic pressure of P_c∼2.3–2.5 kbar [17]. This indicates that in the compound under consideration, the quasiparticles are responsible for the observed large amplitude of the Nernst effect.

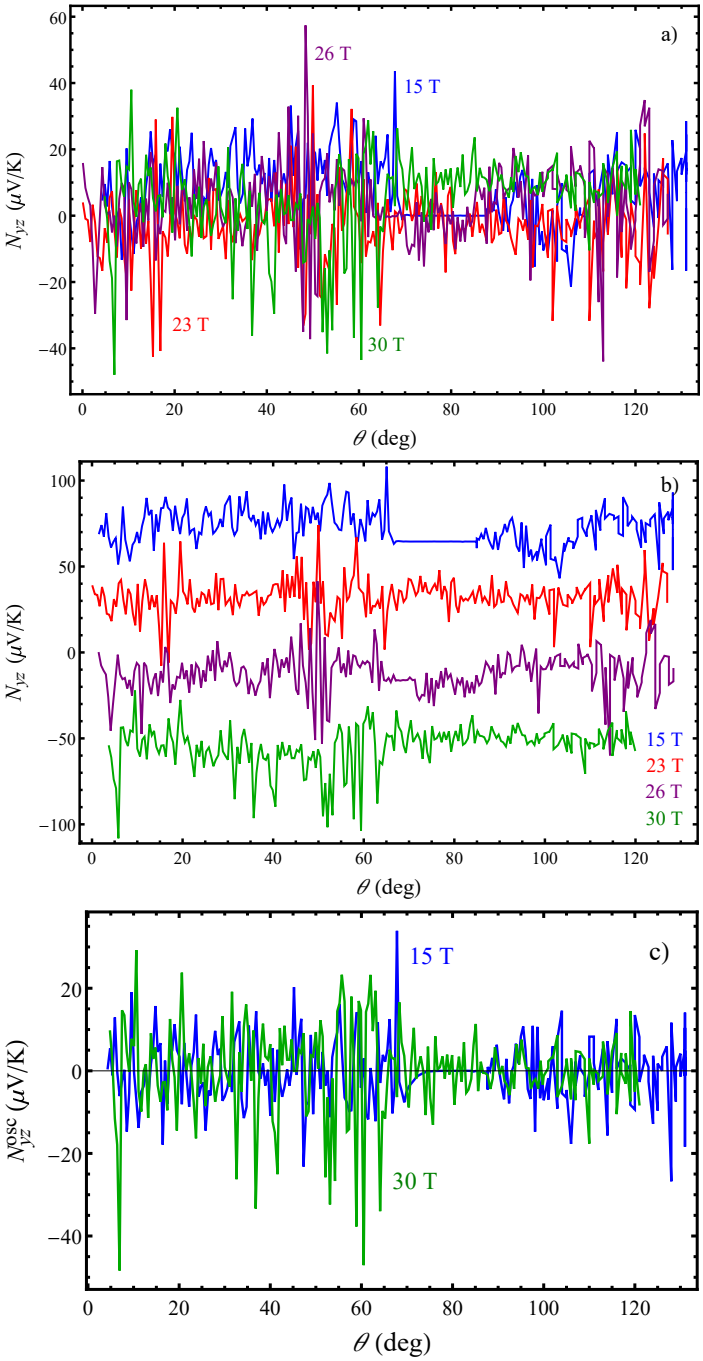

Figure 4. (**a**) Angular oscillations of the total Nernst effect in α-(BEDT-TTF)$_2$KHg(SCN)$_4$ for several fields: $B = 15$ T, 23 T, 26 T and 30 T and $T = 0.6$ K. The Nernst effect quantum oscillations are visible at each magnetic field magnitude in the whole range of angles and are the dominant component in the total Nernst effect. (**b**) The Nernst effect oscillatory curves are shifted for clarity. (**c**) Angular quantum oscillations of the Nernst effect for $T = 0.6$ K at $B = 15$ T and $B = 30$ T differ in amplitude and phase, indicating that the system is driven from one into another CDW state with increasing field and tilt angle.

For obtaining a more detailed picture on the thermoelectric transport in α-(BEDT-TTF)$_2$KHg(SCN)$_4$, one should study the behaviour of the two components, the quantum oscillating component and the background term. The quantum oscillations are visible at each magnetic field magnitude in the whole range of angles. The exceptions are only the angles close to the layer's plane at 15 T in the CDW$_0$ state (Figure 4c) where the total Nernst signal is vanishing, although it should not be zero because the transverse voltage is the largest along the y direction. The quantum oscillations are mainly due to the fundamental frequency of the closed FS α orbit, $F_\alpha = 671$ T, which is present above $B = 8$ T. The oscillatory part of the transport coefficients is determined by the oscillatory dependence of the relaxation time τ that results from the summation over all the electron states in the incoming term of the collision integral. In the Born approximation, for $\hbar\omega_c \ll t_c$, $\tau \sim \tau_0\tau^{\mathrm{osc}}$ where $\hbar$ is the Planck constant divided by 2π, $\omega_c = eB/m^*$ is the cyclotron frequency, m^* is the cyclotron effective mass, t_c is the interlayer transfer integral, and τ_0 and τ_{osc} are the non-oscillatory and oscillatory part of the relaxation time. The oscillatory part of the relaxation time is a sum of the contributions from all extremal orbits, $S_{\mathrm{ext}i} = 2\pi\hbar eF_i$, on the Fermi surface for a particular orientation in a magnetic field $\tau_{\mathrm{osc}} \sim \sum_i A_i(B\cos\theta)^{1/2}R_TR_SR_DR_{\mathrm{MB}}\cos(2\pi(\frac{F_i}{B\cos\theta} - \frac{1}{2}))$, where R_T accounts for finite temperature effects, R_D for impurity scattering, R_S for spin-splitting effects, and R_{MB} for the magnetic breakdown effects. As a result of the oscillatory dependence of τ, the thermoelectric coefficient α_{zz} acquires an oscillatory component $\alpha_{zz}^{\mathrm{osc}} \sim \sigma_0\frac{\partial\tau_{\mathrm{osc}}}{\partial\varepsilon}|_{\varepsilon=\mu}$ and so the oscillatory part of the Nernst effect is $N_{yz}^{\mathrm{osc}} \sim \frac{\alpha_{zz}^{\mathrm{osc}}}{\sigma_{yz}} \sim \frac{1}{\sigma_{yz}}\sum_i A_i(B\cos\theta)^{-1/2}R_TR_SR_DR_{\mathrm{MB}}\sin(2\pi(\frac{F_i}{B\cos\theta} - \frac{1}{2}))$. It is large when a Landau level meets the chemical potential μ and is damped when μ is between two successive Landau levels. The amplitude of the Nernst effect quantum oscillations is much larger than that of the Hall resistance quantum oscillations (about 10^2 times larger) as can be seen by comparing Figures 2 and 4. This is in correlation with the high fundamental frequency of the main oscillations, F_α, for $\mu \gg \hbar\omega_c$ which strongly increases the amplitude of the effect when performing the derivative of the density of states over μ.

The background Nernst effect shown in Figure 5 reveals oscillatory features emphasizing the resonant-like character of the effect. The resonance-like behaviour of the background Nernst effect is evident at each magnetic field magnitude similar to that previously observed in the angular dependence of the Seebeck effect [16]. Apart from that, the angular dependence of the Nernst effect changes significantly with increasing magnetic field strength. This is a reflection of the complex electronic properties associated with the existence of different CDW states in this organic metal. It should be specifically emphasized that all of the Nernst effect curves show different behaviour above a certain tilt angle, $\theta_c \sim 60°$, which corresponds to the second maximum in the Hall resistance angular dependence. At a lower field ($B = 15$ T), when the system is in the CDW$_0$ state, the Nernst effect decreases above θ_c without changing the sign. A decrease in the Nernst effect amplitude is also seen at $B = 26$ T above θ_c accompanied with a sign change around $\theta = 85°$. At $B = 30$ T, the Nernst effect is zero at θ_c above which it is positive with a pronounced increase in the amplitude. For $B = 26$ T and $B = 30$ T, the system is supposed to be in the CDW$_x$ state, but the observed distinct behaviour of the Nernst effect around θ_c implies that this is not the case. The curve obtained for $B = 23$ T demonstrates the most unusual behaviour as the Nernst effect constantly changes sign in the angular range between the first and third AHRO maximum. Most strikingly, the curve is mirroring its angular behaviour exactly at θ_c, which is not characteristic for the other curves. The observed different Nernst effect behaviour, especially above θ_c, with or without a sign change, indicates that significant changes occur in the density of states.

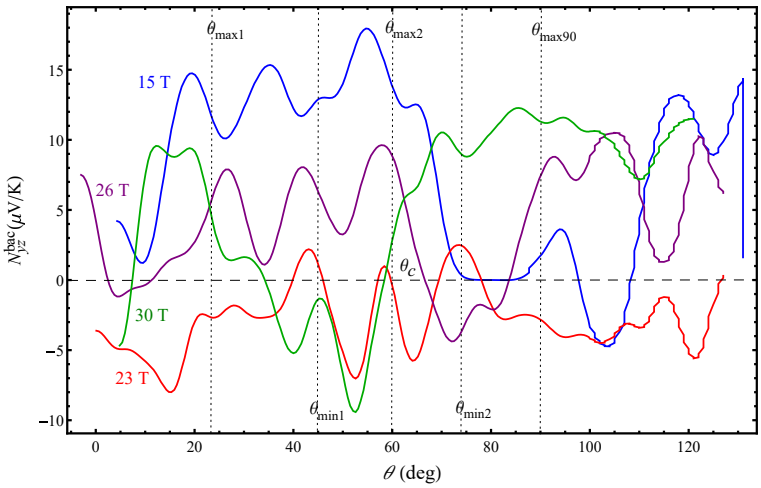

Figure 5. Angular oscillations of the background Nernst effect in α-(BEDT-TTF)$_2$KHg(SCN)$_4$ for several fields: B = 15 T, 23 T, 26 T, 30 T at T = 0.6 K. The positions of some of the AHRO maxima and minima are indicated by the vertical dashed lines.

In order to capture the magnitude of the observed Nernst signal at low temperature, we present in Figure 3 the AMROs, AHROs, Seebeck and Nernst effect angular oscillations at $B = 15$ T and $T = 0.6$ K. It is clearly seen that the amplitude of the Nernst effect is exceeding by far the amplitudes of the other effects with an exception of a small interval of field orientations near the layer's plane where the Nernst signal is zero and the Seebeck effect is the main thermoelectric response, although this should not be observed when the temperature gradient is along the normal to layer's plane. In addition to the large amplitude, there are other features that should be addressed concerning the behaviour of the angular Nernst effect in the CDW state. The features observed in the angular Nernst effect for $T = 0.6$ K neither appear at the magic angles (where the peaks and dips in the AMRO and AHRO are observed) nor are located at the mid angle positions. However, the latter was observed in the Nernst effect angular oscillations for $T = 4$ K [18]. Another interesting observation is that for $T = 4$ K, in the CDW$_0$ state, the Nernst effect is also oscillatory up to angles $\theta_c \sim 60^\circ$ but with a 10 times smaller amplitude than that for $T = 0.6$ K. However, for $T = 0.6$ K, the Nernst effect is the largest in the CDW$_0$ state up to angles $\theta \sim 70^\circ$ (Figure 5). This implies that at low temperatures, deep down in the CDW$_0$, there are some processes that are dominant leading to an existence of a large transverse thermoelectric response in the current compound, and the Nernst effect is very sensitive to these low-temperature processes.

By comparing Figures 2 and 5, one can see that the transverse thermoelectric transport represents more remarkable signatures of the CDW transitions, as the Nernst effect is very different from the Hall resistance. This is because in α-(BEDT-TTF)$_2$KHg(SCN)$_4$, the Nernst effect is especially sensitive to both the Landau-level spectrum and energy gap in the electronic structure. We find that both the quantum oscillating and background component of the Nernst effect behave differently with increasing angles and fields. At $B = 15$ T, the amplitude of the quantum oscillations is of the same order as the background up to angles $\theta_c \sim 60^\circ$, while above this angle, there is a sudden decrease in both components, which vanishes for field orientations close to the plane of the layers. This behaviour, however, is not expected, as the Nernst signal is supposed to be the largest when the generated transverse electric field is the largest. With an increasing field, at $B = 23$ T and $B = 26$ T, the quantum oscillating component is dominant over the background one in the whole range of angles. For $B = 30$ T, the quantum oscillating component is larger only below θ_c. Figure 5 shows that above $\theta_c \sim 60^\circ$, the Nernst effect amplitude is large only at high magnetic fields. In the absence of systematic studies of the Nernst effect in other layered q2D organic systems, one may speculate in several directions concerning the origin of the giant Nernst signal. We first note that due to the change of the quantum

Nernst effect component below and above $\theta_c \sim 60^\circ$, there might be a significant change in the quasiparticle density of states at the Fermi energy, which may lead to an enhanced Nernst signal. On the other hand, the background Nernst effect is intimately related to the off-diagonal component of the thermoelectric coefficient tensor α_{yz}, which is the energy derivative of the off-diagonal conductivity component σ_{yz} at the Fermi energy, according to the Mott formula $\alpha_{yz} = \frac{\pi^2 k_B^2 T}{3e} \frac{\partial \sigma_{yz}}{\partial \varepsilon}|_{\varepsilon=\mu}$. Thus, if σ_{yz} changes due to to a small change in the Fermi surface volume, this could also lead to an enhanced α_{yz} and hence to a sizable Nernst signal. Since the Nernst effect is very sensitive to changes in the Fermi surface, this implies that in α-$(BEDT\text{-}TTF)_2KHg(SCN)_4$, large changes occur in the out-of-plane electronic structure.

With investigation of the magnetic and temperature dependence of the Nernst effect, in addition to the angular dependence, one can obtain information about the possible sources for detection of the large angular Nernst effect in this multiband system. In regard to that, the obtained magnetic field and temperature dependencies of the Nernst effect (discussed below) suggest that the primary source of producing a large Nernst signal is not the change of the quasiparticle density of states but the change of charge carriers relaxation times (i.e., the change of the charge carriers scattering rates). Although the charge relaxation dynamics has not been much considered in studying the thermoelectric effects, in many cases, it can be dominant in producing a sizeable thermoelectric response, especially a transverse one. However, we have detected a large angular Nernst signal in contrast to the observed much smaller magnetic Nernst signal (Figure 6 below). This implies that the observed giant angular Nernst effect is not only due to changes in the density of states and scattering rates but also due to changes in the charge carriers velocity as they move along different parts of the FS. Indeed, with changing the field orientation, the electron trajectories along the corrugated FS also change. For specific field orientations, the velocity is more effectively averaged to zero, and therefore, transport is reduced. For the Fermi cylinder, the velocity vector along the cylinder axis goes to zero when all closed orbits have the same area. For the open Fermi sheets, the velocity vector is reduced when the electrons are not moving along the corrugation axis. This can explain the zero angular Nernst signal observed at certain angles in Figure 5. In addition, the Nernst effect is most clearly manifested when the temperature gradient and the velocity vector of the q1D charge carriers are not perpendicular to each other [19]. This might be the reason for observing the largest angular Nernst effect in the CDW_0 state for angles below θ_c and a zero Nernst effect for angles close to the plane of the layers (blue curve in Figure 5). On the other hand, a large Nernst effect is observed above $\theta_c = 60^\circ$ at a high field (green curve for $B = 30$ T in Figure 5). The Nernst signal is positive and large as a result of the formation of a significant number of new closed hole-like orbits obtained as a result of the magnetic breakdown effect. Considering that a field of 30 T is larger than the magnetic breakdown field ($B_{MB} = 20$ T), many new closed orbits with a different area are formed, and thus, the q2D charge carriers velocity vector, along the cylinder axis, significantly differs from zero. For $B = 26$ T (purple curve in Figure 5), the Nernst effect is resembling that for 15 T for angles below $\theta_c = 60^\circ$ but is not zero for field orientations close to the plane of the layers. It seems that at high fields, the CDW_0 state is still present for angles below θ_c, although the magnetic field for this measurement is larger than the kink field B_K, and the CDW_x state is expected to be observed instead of the CDW_0. However, above θ_c, the system is in the CDW_x state due to the appearance of new electron-like closed orbits resulting from the magnetic breakdown. The peculiar behaviour of the Nernst effect for $B = 23$ T (red curve in Figure 5) is correlated to the proximity of the field (for which this angular dependence is obtained) to the kink field, $B_K \sim 22$ T, at which the $CDW_0 \rightarrow CDW_x$ transition occurs. Therefore, for $B = 23$ T, the Nenst effect curve is most probably a result of the mixing of contributions from several bands, and hence, it reflects the properties of both the CDW_0 and CDW_x state.

With rotation of the magnetic field from the direction of the temperature gradient towards the plane of the layers, the average velocity of charge carriers along the z-axis, $\bar{v}_z$, decreases, but the average velocities along the x- and y-axis, $\bar{v}_x = \bar{v}_z \cos\phi \tan\theta$ and

$\bar{v}_y = \bar{v}_z \sin\phi \tan\theta$, are rather large. This can lead to the generation of a substantial in-plane Nernst signal N_{yx}. In other words, the in-plane Nernst effect component can be significant, and its contribution can not be neglected as it can affect the overall behavior of the out-of-plane Nernst signals due to mixing of the components of the thermoelectric tensor α_{ij}. In support of this scenario, Choi et al. [20] have shown that at low temperatures, the in-plane Nernst effect N_{yx} is large enough even when the magnetic field is applied along the b-axis, i.e., along the direction of the temperature gradient.

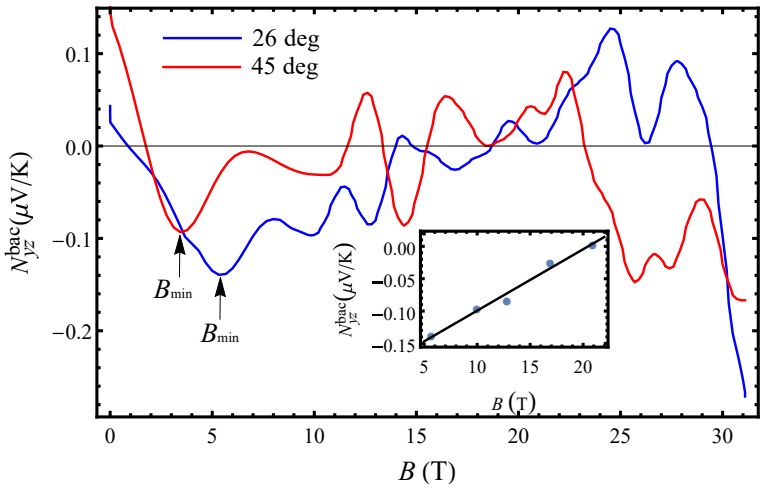

Figure 6. Magnetic field dependence of the background Nernst effect in α-(BEDT-TTF)$_2$KHg(SCN)$_4$, $N_{yz}^{bac}(B)$ after filtering out the quantum oscillation component. The minimum and maximum features that appear in the field dependence at different field orientations are evident. The arrows indicate B_{min}, which is angle-dependent and decreases with the increasing tilt angle. The inset shows the magnetic field dependence of the dip-to-dip amplitude of the Nernst effect at $\theta_{max1} = 26°$.

3.2. Resonant Magnetic Field Nernst Effect

Figure 7a shows the magnetic field dependence of the total Nernst effect in α-(BEDT-TTF)$_2$KHg(SCN)$_4$ obtained at $T = 0.6$ K and $\theta = 26°, 45°$. The angles correspond to the orientations of the magnetic field where the AHROs have a maximum and a minimum (first maximum and minimum in Figure 2), since the Nernst effect behaves differently at these orientations. At low temperatures, the magnetic Nernst effect is small compared to the Seebeck effect [16]. The magnetic Nernst effect has a similar amplitude for orientations corresponding to both the AHRO maximum and minimum. From Figure 7b, which presents the magnetic quantum oscillations of the Nernst effect with the inverse magnetic field, one can see that the total magnetic Nernst effect is dominated by the quantum oscillating component in fields above 8 T. The quantum oscillations are mainly determined by the fundamental α frequency with a small contribution from its second harmonic only for $\theta_{max1} = 26°$. There is no significant change in the amplitude of the magnetic quantum oscillations on crossing the kink field B_K~24 T, i.e., with the transition from CDW$_0$ to CDW$_x$ state. This is opposite from what was observed for the angular quantum oscillations where the amplitude of the oscillations changes significantly depending on if the field, for which a given angular dependence is obtained, is below or above the kink field B_K. This implies that if indeed, there are changes happening in the out-of-plane electronic structure in this organic metal, as suggested by the angular Nernst effect behaviour, then these changes are greatly triggered by the magnetic field rotation and are manifested mostly in the Nernst effect and not in the Seebeck effect (as evident from the large angular Nernst effect in this work and the small angular Seebeck effect in Ref. [16]).

The background Nernst effect shown in Figure 6 also manifests minimum and maximum features in the magnetic field dependence similarly to those previously observed in the background Seebeck effect in Ref. [16]. However, the features seen in the Nernst effect are slightly more pronounced (especially with increasing angle), although the Seebeck effect

is exceeding the Nernst effect. For angles close to the b-axis ($\theta_{max1} = 26°$, corresponding to the first AHRO maximum), the Nernst effect shows weak oscillatory features and changes sign at $B \sim 18$ T and also around $B \sim 30$ T. The electron–hole asymmetry in the CDW_0 state is evident as the transport changes from electron-like to completely hole-like. In the CDW_0 state, the Nernst signal changes significantly at $B_{min} \sim 5$ T from a relatively linear (below B_{min}) to an approximately linear (increase in slope) with field. For $\theta_{max1} = 26°$, the dip-to-dip Nernst effect amplitude changes linearly with field as shown in the inset in Figure 6. The negative Nernst effect below 18 T, in the CDW_0 state, indicates that the transport is essentially electron-like due to the electrons on the open Fermi sheets. This, on the other hand, confirms that the small closed orbits do not form in the CDW_0 state after the Fermi surface reconstruction; i.e., there are only open electron orbits in this state. However, since magnetic breakdown effects take place around $B = 20$ T, the probability for the formation of closed hole orbits is increasing with increasing fields.

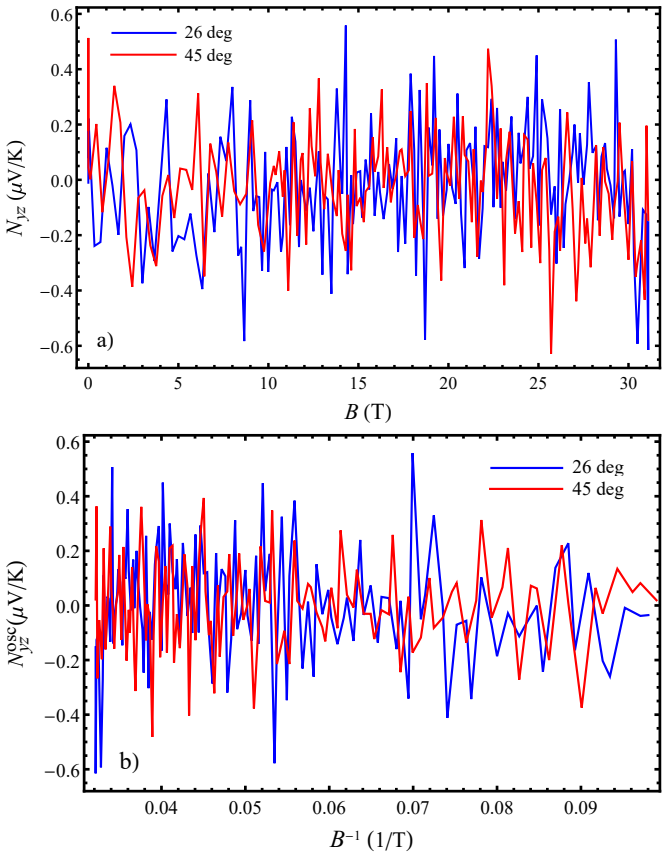

Figure 7. (**a**) Magnetic field dependence of the total Nernst effect in α-$(BEDT\text{-}TTF)_2KHg(SCN)_4$ obtained at $T = 0.6$ K and different angles: $\theta = 26°, 45°$ that correspond to the first maximum and first minimum in the Hall resistance angular oscillations, respectively. (**b**) Magnetic quantum oscillations of the Nernst effect with the inverse magnetic field at the same angles (B is in the range 10–30 T). The quantum oscillations display a complex structure with multiple periodicities.

With tilting the field at the first AHRO minimum ($\theta_{min1} = 45°$), the oscillatory features become more prominent, but the Nernst effect is in general small. An important observation is that when the field is located at the AHRO minimum, the Nernst effect changes sign first at a low field, then in between 10 and 18 T, and again just before entering the high-field CDW_x state where it becomes negative. Above the kink field for this angle, $B_K = 25$ T, the Nernst signal is weakly field dependent, resembling the behaviour of the Seebeck effect but with a smaller amplitude. Here, the field dependence changes from linear to non-linear at $B_{min} \sim 3.5$ T. The sign change in the field range B = 10–18 T is due to the formation of new electron and hole-closed orbits as a result of the magnetic breakdown. In

that way, with increasing angle and field, both types of charge carriers become involved in the thermoelectric transport, while their dominance changes with increasing field. For this field orientation, the closed electron/hole orbits are formed much below the magnetic breakdown field. The different Nernst effect behaviour with the magnetic field from that observed for $\theta_{max1} = 26^\circ$ shows that the q1D charge carriers are not the dominant carriers with increasing angle, but the role of the q2D carriers becomes essential in the transport processes at moderate fields of 10 T.

The charge carrier concentration changes depending on the magnetic field direction (maximum or minimum location). Although the carrier density n is difficult to estimate for the present metal with both open and closed bands, we could obtain $n(\theta_{max1}) = 6.9 \times 10^{18}$ cm^{-3} and $n(\theta_{min1}) = 1.6 \times 10^{18}$ cm^{-3} for $B = 15$ T by using the simple relation $n = 1/eR_H$. Since $n(\theta)$ decreases with the rotation of the field at the location of the first minimum, the amplitude of magnetic Nernst effect quantum oscillations slightly grows, and their frequency becomes smaller (Figure 7b). For these carrier concentrations, giant angular Nernst quantum oscillations with a single frequency are observed. Taking into account that these are not very high carrier concentrations and given that the in-plane conductivity is large, it follows that the carrier mobility, $\mu_B = \sigma/en$, will be high. In addition, as $n(\theta)$ changes with the field rotation from the AHRO maximum to the AHRO minimum, the charge mobility changes rapidly with the rotation of the field from the AHRO maxima to the AHRO minima. We further investigate, with the temperature-dependent measurements of the Nernst effect, what processes contribute to the rapidly changing carrier mobility, which can significantly contribute to the Nernst effect enhancement in the given compound.

3.3. Temperature Dependence of the Nernst Effect

The temperature dependence of the out-of-plane Nernst effect presented in Figure 8 shows that the effect is strongly non-linear in the given temperature range, and the temperature profile changes significantly with increasing field and angle. One striking feature of Figure 8a is the presence of a large negative Nernst signal in the CDW_0 state and an even larger Nernst effect in the mixed state. The Nernst effect has a magnitude drastically exceeding what is expected for a multiband system. A large Nernst effect has been also discovered in some Bechgaard salts for fields oriented along the magic angles [5] and in some heavy-fermion compounds [21]. More interestingly, our results show that the Nernst effect in the organic metal α-(BEDT-TTF)$_2$KHg(SCN)$_4$ has a very similar behavior and size compared to that in a heavy-fermion superconductor $CeCoIn_5$ [22]. This indicates that quasiparticels can lead to a large Nernst signal in the total absence of superconducting fluctuations.

For a magnetic field of 20 T oriented along the first AHRO maximum ($\theta_{max1} = 26^\circ$), the temperature dependence of the Nernst effect shown in Figure 8a reveals there is a CDW_0 state below 8 K with a $N_{yz}(T) = A + B/T + CT^3 + DT^5$ dependence (A, B, C and D are constants). Above 8 K, instead of the expected metallic behaviour, a mixed state with a $N_{yz}(T) = E + FT + GT^3 + HT^5$ dependence (E, F, G and H are constants) is realized. The Nernst signal changes sign from positive to negative around 6 K, indicating a change in the dominant charge carriers in the thermoelectric transport. The observed broad positive and negative maximum in Figure 8a might be an indicator that there is a thermally induced counter-flow of electrons and holes when the field is oriented at the first AHRO maximum. Our results reveal that the temperature profile is complex, as several terms arising from different processes appear in the temperature dependence. The thermal activation over an energy band gap gives a $1/T$ dependence, as expected, since the system is driven into the CDW_0 state. The presence of this term indicates that the electron–phonon coupling has an essential role in the transport processes at low temperatures and high fields. However, only the phonon drag term does not provide a reasonable fit to the data. There are two additional terms in the temperature dependence proportional to T^3 and T^5, respectively. This was not observed in the Seebeck effect temperature profile for the same field magnitude and orientation [16]. The presence of these terms in the given temperature dependence is a clear indicator that the relaxation times (on which the components of the kinetic and

thermoelectric coefficients depend) have different temperature dependence. The absence of the above terms in the Seebeck effect temperature dependence indicates that the Nernst effect is much more sensitive to the change in the relaxation dynamics in this organic metal. The energy relaxation processes governing the electron–phonon interactions and the momentum relaxation processes governing the charge carriers mobility are described by the temperature-dependent scattering times, $\tau_\varepsilon(T)$ and $\tau_p(T)$. The components of the electrical conductivity tensor σ_{ij} depend on τ_p and the components of the thermoelectric coefficient tensor α_{ij} depend on τ_ε. At temperatures much less than the Debye temperature Θ_D, as it is in the case under consideration, the temperature dependence of τ_ε is different than that of τ_p. With the obtained T^3 and T^5 terms in the Nernst effect temperature profile, our results show that the energy and momentum relaxation processes might have an important role in observing the large Nernst signal, especially in the CDW_0 state. For $T \ll \Theta_D$, electron–phonon scattering processes make a significant contribution to the energy relaxation. In that case, τ_ε is proportional to T^3, and the momentum relaxation time τ_p is proportional to T^5 [19]. The presence of the latter term indicates the presence of a significant momentum relaxation dynamics in the CDW_0 state. A significant gradient of charge relaxation processes can generate a sizeable contribution to the transverse thermoelectric signal. The observed temperature dependence of the Nernst effect arises predominantly from the presence of the q1D group of charge carriers in accordance with the picture of a reconstructed Fermi surface with strongly corrugated open Fermi sheets in the CDW_0 state. Thus, except for the phonon drag, the change of the electron scattering rates can lead to an unusually large Nernst effect signal. As already known, peak structures in the temperature dependence of the Nernst effect appear as a result of the phonon drag effect (since the Nernst effect is more sensitive to the phonon drag effect than thermopower), but in this case, the change in the electron scattering rates additionally contributes to the observed large Nernst effect. It is known that the momentum relaxation time is proportional to the charge carrier mobility, $\tau_p = \mu_B e/m^*$. In that way, any change in τ_p will lead to a change in the charge carrier mobility. If τ_p is large enough, then there is a counter-flow of high mobility charge carriers (thermally induced quasiparticles) that contributes to generating a large transverse voltage. This is in agreement with results previously obtained from the angular and magnetic field dependence of the Nernst effect. In that way, in a material with a changing carrier mobility, resulting from changes in the relaxation dynamics, the Lorenz force acting on the slow and fast carriers of the cold and hot ends of the sample will not be fully compensated, which can lead to a sizeable Nernst effect. Above 8 K, instead of observing only a metallic state, there is a mixed state with a non-metallic behaviour in which the CDW_0 state still exists, indicating that the FS is still reconstructed. The phonon drag effect is not affecting the Nernst effect behaviour, but the relaxation processes are not reduced up to $T \sim 12$ K. In the mixed state, the momentum relaxation is adding more to the Nernst signal than the energy relaxation, leading to a peak around 11.8 K.

For a magnetic field of 25 T oriented along the first AHRO minimum $\theta_{\text{min1}} = 45°$ (Figure 8b), the Nernst effect has a significantly smaller amplitude and a $N_{yz}(T) = M + N/T + LT^3$ dependence (M, N and L are constants) below 4.5 K. At this angle and field, the CDW_x state (high field CDW state) is realized in α-$(BEDT\text{-}TTF)_2KHg(SCN)_4$ below 4.5 K. This shows that in the high field state, the Nernst effect is a result of the phonon drag effect and electron–phonon interactions. The absence of the T^5 term for the CDW state excludes the contribution from the momentum relaxation processes in this state. This refers to the decrease in the carriers mobility with increasing angle and field. Above 4.5 K, a non-metallic behaviour is observed, which is characterised with the following temperature dependence $N_{yz}(T) = P + QT + RT^3$ (P, Q and R are constants). This implies that a mixed state showing properties of a weakened CDW_x state and metallic state is realized. Interestingly, mixed states have been also observed in the thermopower temperature dependence when the magnetic field is located exactly at the AMRO maximum or minimum. No mixed state is found when the field is along the normal to the conducting *ac* plane [16]. Obviously, the rotation of the magnetic field away from the temperature gradient direction, at the AMRO (AHRO)

maxima and minima locations, brings the system into some kind of mixed states, which is an indication of a significant change in the electronic structure. The transitions from a pure CDW state into a mixed state occur at different temperature. The apparent trend is that with increasing angles, the transition is reached at a lower temperature. This shows that, most probably, the FS is not completely restored in the given temperature range, indicating that this organic metal has a very complex electron structure that changes depending on the underlying conditions. It seems that the presence of a temperature gradient contributes greatly to these changes by affecting the dynamics and flow of the quasiparticles. The obtained temperature dependencies clearly show that the relaxation processes change when the system transitions from one into another ordered state. Obviously, they are most pronounced in the CDW_0 state (Figure 8a), while they are strongly reduced in the CDW_x state, which is evident from the much smaller Nernst effect amplitude with increasing field and angle (Figure 8b). The predicted Nernst effect behaviour for temperatures outside of the temperature range used in these measurements is seen from the insets in Figure 8. The presented results greatly contribute not only for revision of the previous findings about the thermoelectric transport but also for obtaining information on the possible mechanisms responsible for the existence of different phases in the given organic metal.

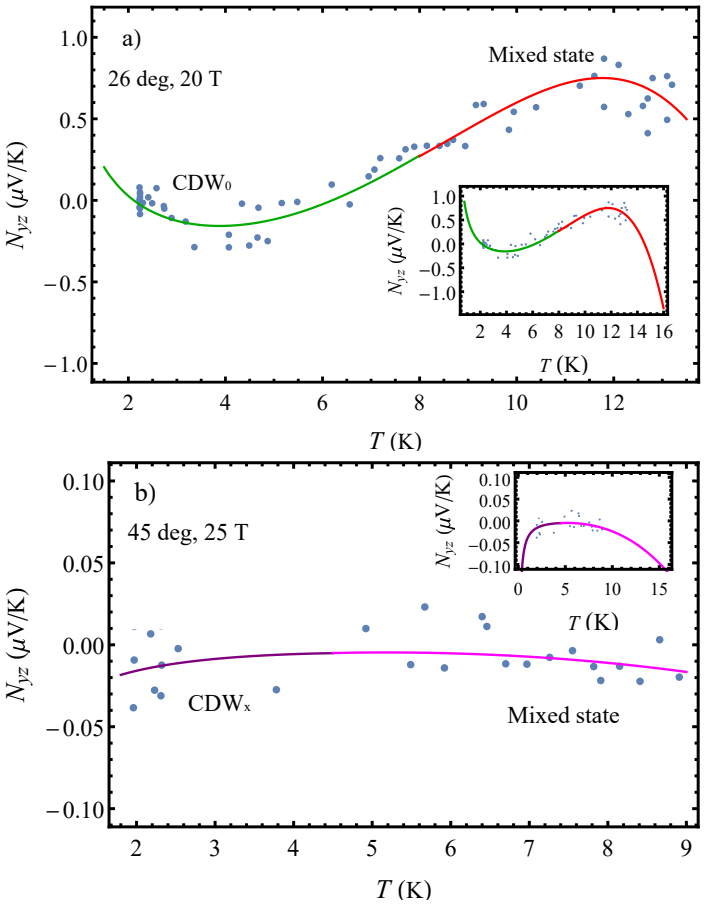

Figure 8. Temperature dependence of the Nernst effect, $N_{yz}(T)$, in α-$(BEDT\text{-}TTF)_2KHg(SCN)_4$ obtained at: (**a**) $\theta = 26°, B = 20$ T and (**b**) $\theta = 45°, B = 25$ T. The prominent change in the temperature profile of Nernst effect is evident with increasing tilt angle and magnetic field strength. The insets show the predicted temperature profile of the Nernst effect outside of the measured temperature range.

4. Conclusions

In conclusion, we report on the study of Nernst effect in the quasi-2D organic metal α-$(BEDT\text{-}TTF)_2KHg(SCN)_4$, showing charge density wave instabilities. The behaviour of the Nernst effect with the angle, magnetic field and temperature is analyzed. We find that

in this multiband system, the transverse thermoelectric response is dominant when the magnetic field is rotated from the least conducting axis towards the plane of the layers. A combination of mechanisms including the phonon drag effect and the relaxation processes can lead to the enhanced Nernst effect with a large amplitude similar to that reported in some quasi-1D organic conductors and heavy-fermion compounds. The energy and momentum relaxation processes have a significant role in observing the largest Nernst signal in the CDW_0 state. The obtained temperature dependence of the Nernst effect when the field is oriented at the location of the first AHRO maximum shows that there is a change in the momentum relaxation dynamics in the CDW_0 state with increasing temperature. The momentum relaxation processes are absent in the CDW_x state for which the main mechanisms are the phonon drag effect and electron–phonon interactions. We suggest that in this organic metal, due to changes in the relaxation dynamics, there is a change in the carrier mobility. When the momentum relaxation time is large enough, then there might be a counter-flow of high mobility quasiparticles that contributes to a generation of a large transverse voltage. Thus, the Lorenz force acting on the slow and fast carriers of the cold and hot ends of the sample will not be fully compensated, leading to a sizeable Nernst effect. The observed giant angular Nernst effect is not only due to the change in the relaxation times and thus in the charge carrier scattering rate but also due to the change in the charge carriers velocity vector (which moves along different parts of the FS) with respect to the temperature gradient direction. Taking into account the change in the direction of the charge carriers' velocity on different FS parts, in relation to the temperature gradient, one can explain the observed specific behaviour of the angular Nernst signal at certain angles.

Author Contributions: Conceptualisation, D.K.; Investigation, D.K., E.S.C. and E.S.; Resources, E.S.C. and E.S.; Writing—original draft, D.K.; Writing—review and editing, D.K. and E.S.C. All authors have read and agreed to the published version of the manuscript.

Funding: This research received no external funding.

Institutional Review Board Statement: Not applicable.

Informed Consent Statement: Not applicable.

Data Availability Statement: Not applicable.

Acknowledgments: This work was performed at the National High Magnetic Field Laboratory, supported by NSF DMR-0654118, by the State of Florida, and by the DOE.

Conflicts of Interest: The authors declare no conflict of interest.

References

1. Behnia, K.; Measson, M.; Kopelevich, Y. Oscillating Nernst-Ettingshausen effect in bismuth across the quantum limit. *Phys. Rev. Lett.* **2007**, *98*, 166602. [CrossRef] [PubMed]
2. Galffy, M.; Freimuth, A.; Murek, U. Unusual Seebeck and Nernst effects in the mixed state of $Bi_{2-x}Pb_xSr_2Ca_2Cu_3O_\delta$. *Phys. Rev. B* **1990**, *41*, 11029. [CrossRef] [PubMed]
3. Alexandrov, A.; Zavaritsky, V. Nernst effect in poor conductors and in the cuprate superconductors. *Phys. Rev. Lett.* **2004**, *93*, 217002. [CrossRef] [PubMed]
4. Wu, W.; Lee, I.J.; Chaikin, P.M. Giant Nernst effect and lock-in currents at magic angles in $(TMTSF)_2PF_6$. *Phys. Rev. Lett.* **2003**, *91*, 056601. [CrossRef] [PubMed]
5. Wu, W.; Ong, N.P.; Chaikin, P.M. Giant angular-dependent Nernst effect in the quasi-one-dimensional organic conductor $(TMTSF)_2PF_6$. *Phys. Rev. Lett.* **2005**, *72*, 235116. [CrossRef]
6. Choi, E.S.; Brooks, J.S.; Kang, H.; Yo, Y.J.; Kang, W. Resonant Nernst effect in the metallic and field-induced spin density wave states of $(TMTSF)_2ClO_4$. *Phys. Rev. Lett.* **2005**, *95*, 187001. [CrossRef] [PubMed]
7. Kartsovnik, M. High magnetic fields: A tool for studying electronic properties of layered organic metals. *Chem. Rev.* **2004**, *104*, 5737–5781. [CrossRef] [PubMed]
8. Kartsovnik, M. Layered Organic Conductors in Strong Magnetic Fields. In *The Physics of Organic Superconductors and Conductors*; Lebed, A., Ed.; Springer: Berlin/Heidelberg, Germany, 2008; pp. 185–246.

9. Osada, T.; Yagi, R.; Kawasumi, A.; Kagoshima, S.; Miura, N.; Oshima, M.; Saito, G. High-field magnetotransport and Fermi-surface topology in the novel quasi-two-dimensional organic conductor bis(ethylenedithiolo)tetrathiafulvalenium mercuric postassium thiocyanate, $(BEDT\text{-}TTF)_2KHg(SCN)_4$. *Phys. Rev. B* **1990**, *41*, 5428.
10. Sasaki, T.; Toyota, N. Anisotropic galvanomagnetic effect in the quasi-two-dimensional organic conductor α-$(BEDT\text{-}TTF)_2KHg(SCN)_4$, where BEDT-TTF is bis(ethylenedithio) tetrathiafulvalene. *Phys. Rev. B* **1994**, *49*, 10120.
11. Qualls, J.S.; Balicas, L.; Brooks, J.S.; Harrison, N.; Montgomery, L.K.; Tokumoto, M. Competition between Pauli and orbital effects in a charge-density-wave system. *Phys. Rev. B* **2000**, *62*, 10008.
12. Uchida, K.; Konoike, T.; Osada, T. Angle-dependent magnetoresistance oscillations and magnetic breakdown in α-$(BEDT\text{-}TTF)_2KHg(SCN)_4$. *Phys. B* **2010**, *405*, S221–S223.
13. Uchida, K.; Yamaguchi, R.; Konoike, T.; Osada, T.; Kang, W. Angle-dependent magnetoresistance oscillations and charge density wave in the organic conductor α-$(BEDT\text{-}TTF)_2KHg(SCN)_4$. *J. Phys. Soc. Jpn.* **2013**, *82*, 043714.
14. Choi, E.S.; Brooks, J.S.; Qualls, J.S.; Song, Y.S. Low-frequency method for magnetothermopower and Nernst effect measurements on single crystal samples at low temperatures and high magnetic fields. *Rev. Sci. Instrum.* **2001**, *72*, 2392. [CrossRef]
15. Brown, S.E.; Chaikin, P.M.; Naughton, M.J. La Tour des Sels de Bechgaard. In *The Physics of Organic Superconductors and Conductors*; Lebed, A.G., Ed.; Springer: Berlin/Heidelberg, Germany, 2008; pp. 49–88. [CrossRef]
16. Krstovska, D.; Choi, E.S.; Steven, E. Seebeck effect studies in the charge density wave state of organic conductor α-$(BEDT\text{-}TTF)_2KHg(SCN)_4$. *Phys. Scr.* **2021**, *96*, 125734. [CrossRef]
17. Andres, D.; Kartsovnik, M.V.; Biberacher, W.; Neumaier, K.; Müller, H. Direct evidence for superconductivity in the organic charge density wave compound α-$(BEDT\text{-}TTF)_2KHg(SCN)_4$ under hydrostatic pressure. *J. Phys. IV* **2002**, *12*, Pr9–Pr87. [CrossRef]
18. Krstovska, D.; Choi, E.S.; Steven, E.; Brooks, J.S. The angular magnetothermoelectric power of a charge density wave system. *J. Phys. Condens. Matter* **2012**, *24*, 265502. [CrossRef]
19. Galbova, O.; Kirichenko, O.V.; Peschansky, V.G. Thermoelectric effect in layered conductors at low temperatures. *Low Temp. Phys.* **2009**, *35*, 810–814. [CrossRef]
20. Choi, E.S.; Brooks, J.S.; Qualls, J.S. Magnetothermopower study of the quasi-two-dimensional organic conductor α-$(BEDT\text{-}TTF)_2KHg(SCN)_4$. *Phys. Rev. B* **2002**, *65*, 205119.
21. Yang, Y.-F. Universal behavior in the Nernst effect of heavy fermion materials. *Phys. Rev. Res.* **2020**, *2*, 033105. [CrossRef]
22. Bel, R.; Behnia, K.; Nakajima, Y.; Izawa, K.; Matsuda, Y.; Shishido, H.; Settai, R.; Onuki, Y. Giant Nernst Effect in $CeCoIn_5$. *Phys. Rev. Lett.* **2004**, *92*, 217002. [CrossRef]